ELSEVIER

Materials Science and Engineering A360 (2003) 356–364

MATERIALS SCIENCE & ENGINEERING A

www.elsevier.com/locate/msea

Investigation of interfacial segregation at antiphase boundaries in a ternary alloy 84.8Ni–12.8Al–2.4Ta

C.Y. Chen [a,*], R. Schäublin, W.M. Stobbs [b]

[a] *Institute of Nuclear Energy Research (INER), P.O. Box 3-14, 1000 Wenhua Road, Chiaan Village, Lungtan, Taiwan*
[b] *Department of Materials Science and Metallurgy, University of Cambridge, Cambridge CB2 3QZ, UK*

Received 31 January 2003; received in revised form 31 May 2003

Abstract

A thin interphase layer ($\sim$4 nm) between the merging γ' precipitates in a chosen model alloy 84.8Ni–12.8Al–2.4Ta was investigated. It is demonstrated that interfacial segregation may occur at an antiphase boundary (APB) interface between the thin layer and one of the merging γ' precipitates. The magnitude of the lattice displacement (about 1/10[010]) caused by interfacial segregation has been measured both by comparing experimental images with computer simulations, and from high resolution electron microscopy (HREM) fringe spacings using linear regressional analysis. These measurements show a consistent lattice spacing reduction across the APB. Image simulations also highlight the way that the contrast of the bounding partial dislocation affects the APB interface image and can be used to obtain the lattice shift across the interface when the segregation effects on α-fringe contrast are significant.

Keywords: Segregation; Antiphase boundary (APB); Superalloys; Computer simulations; High resolution electron microscopy (HREM)

1. Introduction

One of the most characteristic high temperature microstructure features of the superalloys is the rapid directional coarsening of the cuboidal γ' precipitates with or without the influence of an applied stress [1,2]. Since the mechanical properties are strongly dependent on the morphology of the γ' precipitates, it is important to understand the effects of alloy elements on the coarsening, which can be related to interfacial reactions between the γ' precipitates. This suggests that interfacial segregation may occur and its effect therefore deserves investigation. However, very little attention has been given to solute segregation to the interface between merging γ' precipitates. This is due to the fact that interfacial segregation is so localized that it is not readily accessible for analysis by conventional analytical techniques.

While demonstrated in previous study that segregation of heavy elements can occur at complex stacking fault (CSF) interfaces in a typical commercial IN-738LC superalloy [3], it is the objective of this study to investigate whether there is interfacial segregation at an antiphase boundary (APB) in γ/γ' alloys. This would allow also us to rationalize the mechanism of the interfacial segregation and directional coarsening behavior of γ' in γ/γ' alloys. The analytical transmission electron microscopy (TEM) techniques such as using Burgers vector analysis, computer simulations, high resolution electron microscopy (HREM) and regressional analyses are applied not only to characterize the contrast behavior of interfaces in γ' particles, but also to quantify the lattice displacement across the interface. To our best knowledge, this is the first time that the magnitude of the lattice displacement caused by compositional segregation in γ/γ' alloys has been directly measured.

* Corresponding author. Fax: +886-3-471-1409.
E-mail address: cychen@iner.gov.tw (C.Y. Chen).

0921-5093/03/$ - see front matter © 2003 Elsevier B.V. All rights reserved.
doi:10.1016/S0921-5093(03)00478-7

2. Experimental

A ternary model material with nominal composition of Ni–21Al–4Ta was supplied by Rolls Royce. Since no γ–γ' interfaces were observed in the as-received material Ni–21Al–4Ta in the TEM, samples of Ni–12.8Al–2.4Ta were made (from 11.17 g of Ni–21Al–4Ta with the addition of 7.5 g of 99.99% Ni) by arc-melting in an argon atmosphere in order to produce a γ/γ' alloy. The composition of the material after homogenization was then checked by EDX analysis, both on bulk samples in a SEM and on thin foils in a TEM. The results for Ni–12.8Al–2.4Ta are listed in Table 1 and are close to the nominal composition. In order to avoid significant microsegregation, most of the TEM studies were carried out after homogenization. The samples were sliced and evacuated in quartz tubes to $< 5 \times 10^{-5}$ torr, backfilled with $\sim$600 torr argon and then sealed under argon. The encapsulated samples were used for heat-treatment.

The Ni–12.8Al–2.4Ta specimens were solution treated at 1300 °C for 4 days, air-cooled to 1100 °C and held there for 4 h, before finally quenching them in ice water. In order to produce many γ–γ' interfaces for investigation, some as-quenched samples were further heat treated at 1000 °C for 8 days and then water quenched. The samples for TEM were first mechanically ground to $\sim$150 μm thickness using standard metallography techniques and then punched to produce 3 mm discs using a Gatan mechanical punch. After the discs had been punched, they were further ground to a thickness of 60–80 μm and twin-jet polished using a 20% perchloric acid/80% ethanol solution at 36 V and 0 °C. TEM examination was performed on a JOEL 4000EX and a JOEL 2000FX.

BF images of an interface and its bounding dislocation in a γ/γ' alloy were computed using a program written by Schäblin and Stadelmann [4] who have extended a two beam program developed by Head et al. [5] to include both many beams for calculation of images with up to three planar faults and four dislocations, as well as anisotropic elasticity. The program was used following its success in weak-beam studies, e.g. Hemker and Mills [6]. By convention, the beam direction B is parallel to but opposite to the direction of electron flux.

The use of regressional analysis to measure the rigid shift across an interface will be applied using a one dimensional (1D) approach, as described by Dunin Borkowski and Stobbs [7].

3. Results

3.1. General observations

Fig. 1(a) shows the morphology of γ' in the sample which was ice-water quenched after homogenization for 4 days at 1300 °C, air-cooling to 1100 °C and holding for 4 h. As can be seen from the microstructure imaged using a superlattice reflection, the γ' precipitates have remained completely cuboidal and there is apparently no evidence for the onset of rafting. After further annealing the as-quenched sample at 1000 °C for 8 days followed by water-quenching, the microstructure of this alloy reveals γ' precipitates which are directionally coarsened and which have aligned themselves parallel to $\langle 100 \rangle$ cube directions, as shown in Fig. 1(b). It has been generally recognized that the reason for γ' rafts usually lying along $\langle 100 \rangle$ cube directions is that the elastic interaction energy has a negative minimum value when the two particles adjacent to each other are elongated along $\langle 100 \rangle$ directions [8].

In order to find whether there is segregation at interfaces in this chosen model alloy 84.8Ni–12.8Al–2.4Ta, extensive investigations have been carried out on the interfaces formed within the elongated γ' rafts. Various types of interfaces in the γ' during coarsening were observed. This is evident in Fig. 2, where at C the complete coalescence of γ' has occurred and left no defect, whereas at E there is an interface between the γ' precipitates because of the presence of an APB preventing this coalescence. At D, it is remarkable that an isolated dislocation is present at the edge of an interface within the γ', and this separates the region where coalescence of the γ' precipitates has occurred from where it has not. Tilting the specimen from the [011] pole to the [001] pole allowed the interfaces between the γ' precipitates to be viewed edge-on. The thin γ-like layers lying on (010), with a width of about 4nm can be seen in the image in Fig. 2(b) formed using a $2\bar{1}0$

Table 1
Compositional analysis of γ, γ' and $\gamma+\gamma'$ for the Ni–12.8Al–2.4Ta alloy, using EDX in the TEM and SEM

Element	EDX in TEM						EDX in SEM					
	γ		γ'		Av. alloy ($\gamma+\gamma'$)		γ		γ'		Av. alloy ($\gamma+\gamma'$)	
	wt.%	at.%	wt.%	at.%	wt.%	at.%	wt.%	at.%	wt.%	at.%	wt.%	at.%
Ni	89.3	87.3	77.3	79.2	85.7 (86.4)	85.6 (84.8)	90.0	88.0	77.6	79.5	88.4 (86.4)	86.9 (84.8)
Al	5.1	10.9	7.0	15.6	5.3 (6.0)	11.5 (12.8)	4.9	10.4	6.9	15.3	5.1 (6.0)	11.0 (12.8)
Ta	5.6	1.8	15.7	5.2	9.0 (7.6)	2.9 (2.4)	5.1	1.6	15.5	5.2	6.5 (7.6)	2.1 (2.4)

The numbers in parentheses are nominal values from the manufacture of the Ni–12.8Al–2.4Ta alloy.

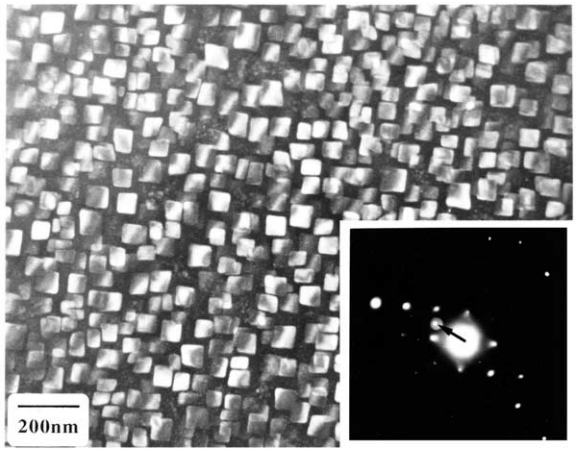

(a)

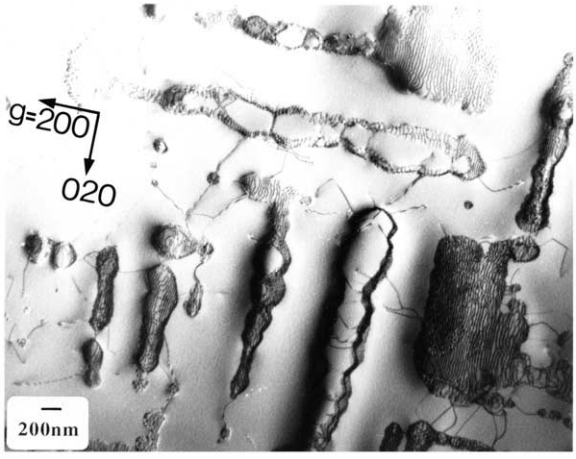

(b)

Fig. 1. (a) TEM dark-field image taken using a superlattice reflection near to the [001] pole, showing small cuboidal coherent γ' precipitates in the sample that had been ice-water quenched after homogenization for 4 days at 1300 °C, then air-cooled to 1100 °C and held for 4 h. (b) After aging at 1000 °C for 8 days subsequent to the heat treated condition shown in (a), the morphology of the γ' shows preferential alignment along $\langle 100 \rangle$ cube directions.

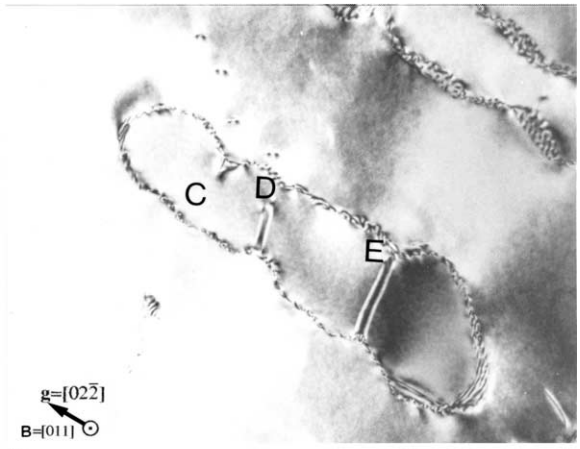

(a)

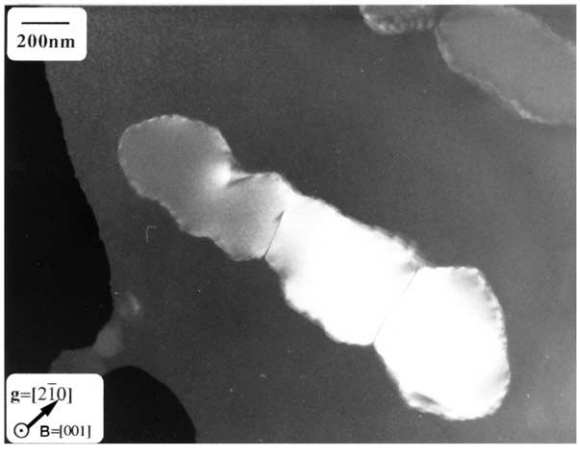

(b)

Fig. 2. (a) $0\bar{2}2$ BF near to (011) showing various interfaces within an elongated γ' precipitate (for details see text). (b) DF images of the same defects but now near to (001) with the interfaces viewed edge-on. Note that a thin interphase layer with a width of about 4 nm can be seen using a superlattice reflection.

superlattice reflection. These thin γ-like layers were however demonstrated to exhibit some short-range ordering in Section 3.5, and will thus be called thin interphase layers hereafter, rather thin γ-like layers or γ-channels.

3.2. Burgers vector analysis

Table 2 gives the **g.b** values of all possible dislocations encountered in γ' for the principal reflections used in the Burgers vector analysis. The Burgers vector of the defect at D in Fig. 2 has been analyzed using the invisibility criterion $\mathbf{g.R} = n$ for faults and $\mathbf{g.b} = 0$ for superpartial dislocations. The results for different diffraction conditions can be seen in Fig. 3. The crystallographic orientations of the operating reflections relative to the interface plane were determined from a comparison

Table 2
Values of **g.b** for possible superpartial dislocations encountered in γ', and for principal reflections obtained at [001], [$\bar{1}$01] and [011] orientations

Fault plane	**b**	**g.b** values for the following **g**				
		g =				
		$\bar{2}00$	020	$0\bar{2}2$	$\bar{1}\bar{1}1$	$1\bar{1}1$
{111}	1/6⟨112⟩	±1/3				
	1/3⟨111⟩	±2/3				
	1/3⟨211⟩	±4/3				
	1/2[$\bar{1}\bar{1}$0]	1	−1	1	1	0
	1/2[$\bar{1}$10]	1	1	−1	0	−1
	1/2[101]	−1	0	1	0	1
	1/2[10$\bar{1}$]	−1	0	−1	−1	0
	1/2[011]	0	1	0	0	0
	1/2[01$\bar{1}$]	0	1	−2	−1	−1

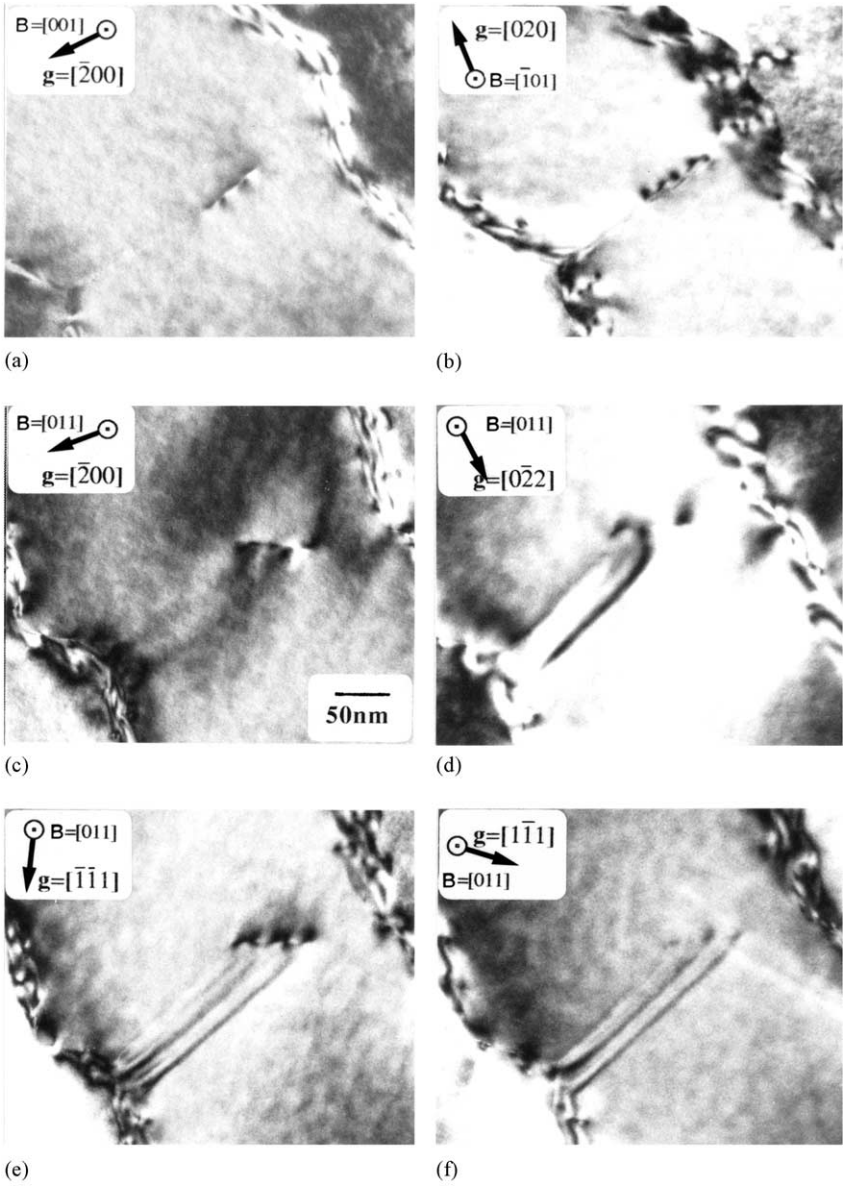

Fig. 3. DF images of the superpartial dislocation marked D in Fig. 2 taken using various reflections and beam directions.

between the images and the corresponding selected-area diffraction patterns (SADP) when tilting from the [001] to the [011] and [$\bar{1}$01] poles. It is clear that the superpartial dislocation is of the type 1/2⟨110⟩ rather than 1/6⟨112⟩, 1/3⟨111⟩ or 1/3⟨211⟩, since the images taken using the reflection $\mathbf{g} = [\bar{2}00]$ reveal near invisible interface contrast, as can be seen in Fig. 3(a and c). (If it were not of the type 1/2⟨110⟩, the interface would be visible due to $\mathbf{g}.\mathbf{R} \neq n$, where n is an integer). Furthermore, the bounding superpartial dislocations are visible using $\bar{2}00$, 020, and $0\bar{2}2$ reflections as observed in Fig. 3(a–d). When these contrast characteristics are compared with the values of **g.b** in Table 2, it is suggested that two kinds of Burgers vector, $(\pm)1/2[110]$ and $(\pm)1/2[\bar{1}10]$, are possible. The latter is excluded simply because the superpartial dislocation is visible using $\mathbf{g} = [\bar{1}\bar{1}1]$ and is almost out of contrast for $\mathbf{g} = [1\bar{1}1]$, as demonstrated in Fig. 3(e and f). Therefore, the Burgers vector of the dislocation is 1/2[110] or 1/2[$\bar{1}\bar{1}$0], which can be differentiated (with respect to the beam direction) using an image-matching technique in Section 3.3. Since the line direction of the dislocation is close to [101], as deduced from trace analysis, this superpartial dislocation is a 60° mixed dislocation and its slip plane, defined as the plane which contains both the dislocation line and the Burgers vector, is ($\bar{1}$11). The Burgers vector of this dislocation is consistent with the observation reported in other superalloys [9].

3.3. Computer simulations

In order to determine the sense of the Burgers vector with respect to the inclination of the fault plane and the magnitude of the lattice displacement due to the thin layers of the interphase lying on (010), bright-field image matching for the same defect shown in Fig. 3 was performed. The general input parameters used for image simulations are given in Table 3. The results of comparisons of the bright-field micrograph with the computer simulations associated with a dislocation of $\mathbf{b} = 1/2[\bar{1}\bar{1}0]$ and various translation displacements **R** from 1/4[010] to 1/15[010] are shown in Fig. 4 for the diffracting condition $\mathbf{g} = [02\bar{2}]$ and a beam direction close to the [011] pole. Since the interface is bounded by a superpartial dislocation which can influence the α-fringe contrast of the interface, the change in the main features of the overall combined image with the translation displacement **R** can be qualitatively used to determine the **R** value of the interface relative to the **b** value of its bounding partial dislocation. It is seen that the lattice translation displacement caused by the interface between γ′ particles is about 1/10[010]. The data used for the image simulations in Fig. 4 are described in Ref. [10]. It should be noted that the lattice displacement has been assumed to be confined to within a single fault plane in all of the simulations presented above. Since the top half of the crystal is considered to be fixed, then the bottom half can be described by the lattice displacement vector **R**. If **R** is pointing upwards (as 1/10[010] in this case), it is regarded as a contraction caused by interface. It is also important to note that the contributions of displacements other than the [010] component to the interface contrast have been ignored, as the interface is nearly out of contrast using 200 and 202 reflections. This indicates that the displacement is parallel to the direction given by 200×202 (i.e. [010]). Whether the approximately 1/10[010] displacement has its origin in compositional segregation or in other effects such as a lattice misfit between a thin interphase layer and the γ′ will be clarified in Sections 3.4 and 3.5

3.4. Lattice misfit

In γ/γ′ alloys in which the precipitation of a γ′ phase with a different lattice parameter from the parent γ phase is observed, it may be possible to measure this difference in lattice parameter from the magnitude of diffraction spot splitting in SADP. Although convergent-beam electron diffraction (CBED) can be used to give more accurate changes in lattice parameter in localized areas, the fact that the observed distortions between γ and γ′ may be caused by stresses associated with thermal and surface relaxation in a thin foil encourage the use of the selected area diffraction pattern (SADP) technique. This method has adequate accuracy and can quickly provide an average lattice misfit by simply placing a SADP aperture on small areas of γ and γ′. In the present study, GaAs was used to provide a standard lattice parameter (5.653 Å) to calibrate the microscope camera constant in situ in the TEM ($\lambda L = rd$ where r is the distance from the transmitted to the diffracted spot on the plate, λ is the electron wavelength, and d is the interplanar spacing of the (hkl) plane). The lattice parameter misfit between γ and γ′ can be obtained by simply measuring the separation of their respective reflections from high order spots taken with large camera lengths (120 and 250 cm was used here). Two typical γ′ precipitates with preferred growth directions of [100] and [010] in a sample of Ni–12.8Al–2.4Ta, which was water quenched after aging at 1000 °C for 8 days, were examined. The position of the SADP aperture with a diameter of ~0.5 μm, from which the SADPs were obtained, will cover γ and γ′. The measured lattice parameters for the (100) and (010) planes are larger for γ′. The result shows that slight additions of Ta will increase the lattice parameter of the γ′ phase and a positive lattice misfit of about 0.6% at the γ–γ′ interface was obtained. This is consistent with the positive misfit observations in Ni–15Al–2Ti–2Ta obtained from X-ray measurements, as made by Pollock and Argon [11]. The measurement of dislocation spacings (about 400–500 Å) at the γ–γ′ interface indicates a misfit of about 0.5–0.6% at room temperature, which is also in good agreement with the SADP measurement. Considering that the coefficient of thermal expansion for the γ phase is greater than for the γ′ phase [12,13], the positive misfit should be maintained but become smaller at an aging temperature of 1000 °C. It should be noted that the lattice misfit (~0.6%) at γ–γ′ interfaces between the γ′ precipitates and the γ matrix cannot be representative of the lattice misfit between the precipitates and the thin interphase layer in between them. This is because the effects of coherent strain at the interfaces may well affect the chemistry in the thin layer and thus change the lattice parameter. This argument is based on the observation that misfit dislocations are absent at the thin interphase layers between merging precipitates, while the non-merging interfaces are populated with a significant density of misfit dislocations as described above.

Table 3
General input parameters for image simulations

Elastic constants: $C_{11} = 222.8$; $C_{12} = 147.9$; and $C_{44} = 125$ GPa[a]
Crystal structure: Ni_3Al
Anomalous absorption: 0.05; Line direction: [101]; Burgers vector: 1/2[$\bar{1}\bar{1}$0]
Foil thickness: 70 nm; Foil normal: [013]; Fault normal: [010]

[a] Taken from the work of Hemker and Mills [6].

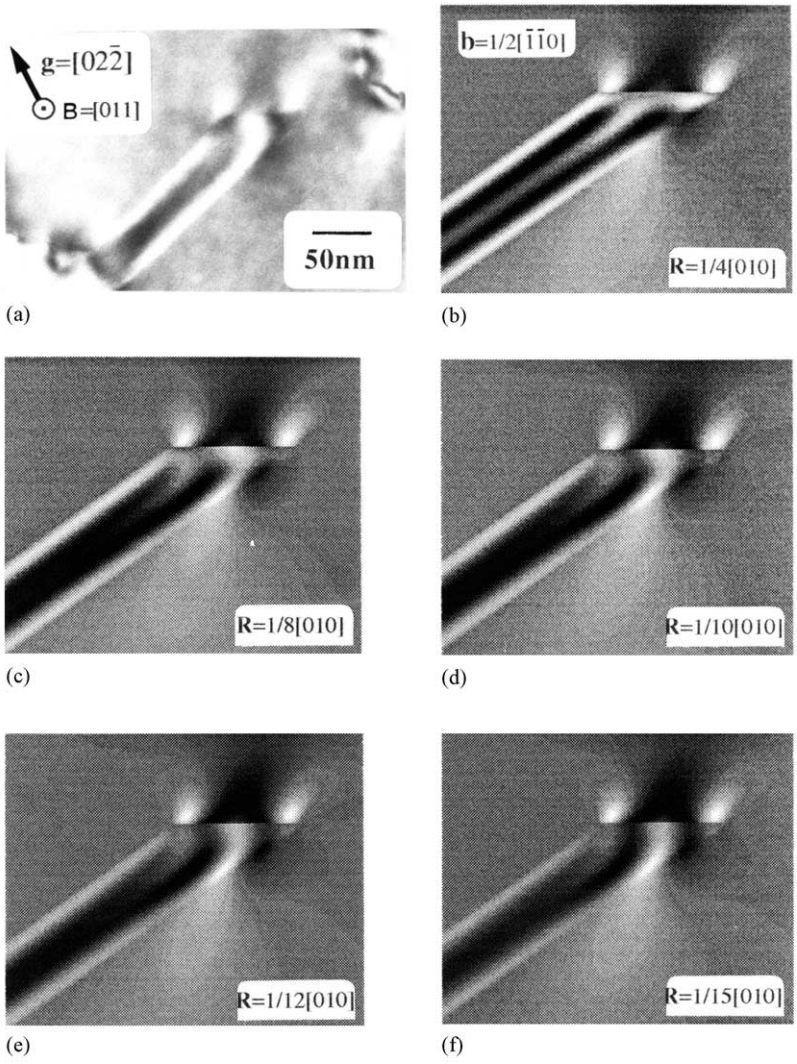

Fig. 4. Qualitative comparison of the contrast characteristics of the experimental micrograph shown in (a) with those of computed images associated with different magnitudes of **R** in (b–f), indicating an approximate translational displacement of 1/10[010].

3.5. HREM images

A thin layer between the merging γ' precipitates was imaged edge-on by HREM for the determination of a rigid body displacement (RBD) across the thin interphase layer as shown in Fig. 5(a). The rigid-body displacement of one γ' precipitate relative to the other can have components both perpendicular and parallel to the interface, and it is the former which can be caused by segregation. In order to determine whether there is a RBD across the interface between two the merging γ' precipitates, the image was digitized in a region where the contrast changes were small between the γ' precipitates on either side of the interphase layer, using a SCANDIG densitometer as described by Ross and Stobbs [14]. The intensity profiles parallel to the (020) lattice fringes were then summed, averaged, and smoothed by convoluting with Gaussians to produce 1D fringe profiles, as shown in Fig. 5(b). Linear regressional analysis of the relative fringe spacings and positions was used to fit the positions of the peaks to leave uncertainties associated with the fringe contrast variation of less than 2% of the d_{020} spacing [7,15]. Using this technique the fringe spacings and positions of peaks in the γ' region on the left-hand side of the image were first fitted (see the enlarged boxed region in Fig. 5(c)), lines of equal spacing (i.e. the positions of lattice planes) were then plotted across the interface, and extrapolated to the γ' region on the right-hand side. The γ' region to the right of the interface is apparently displaced towards the region on the left, as can be seen from the superposition of the two lattices in the boxed region on the right-hand side in Fig. 5(c). The approach taken in this analysis allows the calculation of the relative RBD of the two lattices. A graph of the lattice shift (described as a % of the d_{010} spacing) as a function of fringe position is plotted in Fig. 5(d), from which it is apparent that the lattice shift of the two γ' precipitates

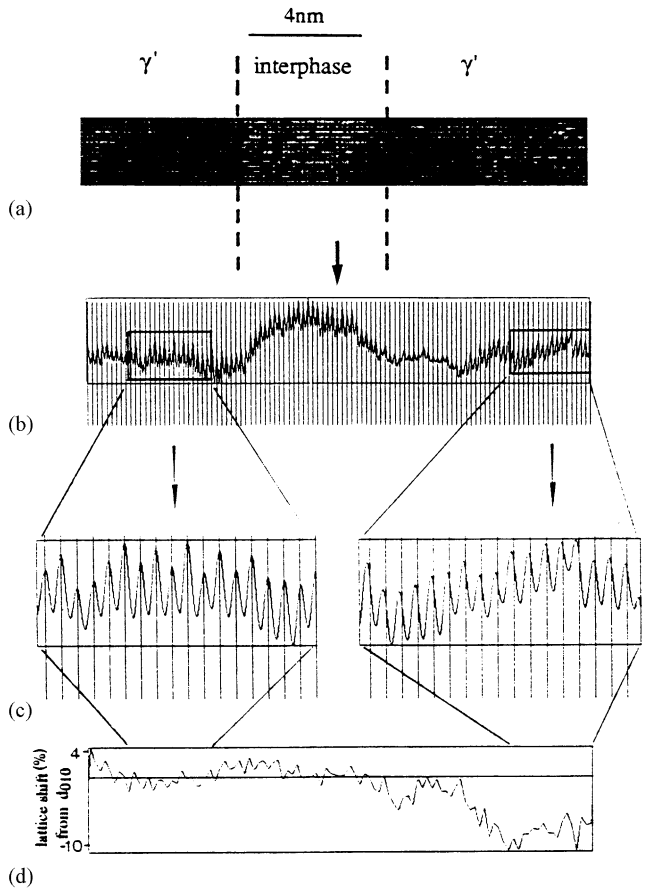

Fig. 5. (a) A digitized region across a thin interphase layer between the merging γ' precipitates. (b) The (020) lattice fringe profile projected in the direction of the arrow. (c) An enlargement of the marked regions in (b) showing disregistry of the two lattices crossing the interphase layer. (d) A graph showing the lattice shift (%) from the d_{010} spacing as a function of fringe position.

on crossing the interface is about 10%. It is of specific interest that there is a significant contraction of the lattice on and near to one side of the phase boundary rather than it being linearly spread across the thin interphase layer. This interesting phenomenon may be associated with the presence of a degree of ordering in the thin interphase layer. Evidence for this partial ordering in the interphase region between the two merging γ' precipitates is shown in Fig. 6; the 1D fringe profile projected in the direction perpendicular to the interphase layer clearly shows short-range ordering in the interphase region, where the oscillating intensity of the (020) lattice fringes in some regions behaves in the same way as that in the γ' precipitates and in phase with the lower γ' in Fig. 6. This is demonstrated by comparison of the weak–strong fringe intensities at the fringe position indicated by the dashed line in Fig. 6(b). Note that it was at the interface with the upper γ' particle, where there is thus an APB, that the displacement appears to be concentrated. It thus appears that the APB for the interface is localized between the thin

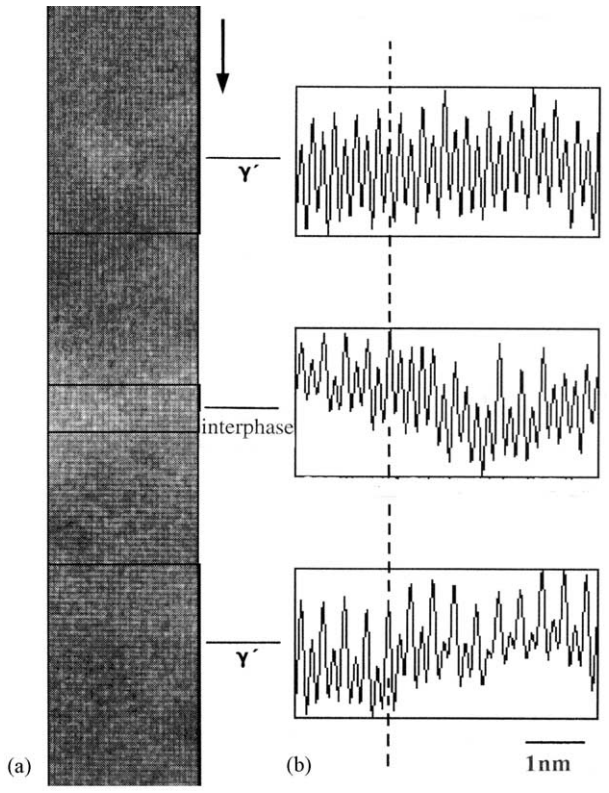

Fig. 6. (a) A digitized region across a thin layer between the merging γ' precipitates. (b) Fringe profiles projected in the direction of the arrow taken from the regions shown in (a), showing the existence of an APB between the merging γ' precipitates.

interphase layer and the upper of the γ' precipitates. That there is a contraction here suggests that this APB interface could be associated with compositional segregation, to give the significant lattice shift across it.

4. Discussion

The results of the above experiments on the Ni–12.8Al–2.4Ta model alloy strongly indicate that interfacial segregation is closely linked to the APB interface and not solely due to a misfitting lattice parameter between the thin interphase layer and the γ' precipitate. The lattice parameter of the matrix γ was found to decrease relative to that of the γ' by about 0.6%, which might produce a lattice shrinkage in a thin layer of γ that has a thickness of only 4 nm. However, the displacement appears experimentally to be localized at one boundary. A smaller lattice shrinkage would be produced in a thin interphase layer given its tendency to short-range ordering. Because there is no external applied stress and the only stresses present are due to thermal stresses and surface relaxation, the contraction of the lattice is probably associated with interfacial segregation at the APB interface. This is suggested by the direct measurement of the lattice shift from the

HREM image which showed that the changes in lattice parameter are mainly confined to the phase boundary between the thin interphase layer and one of the two γ' precipitates. Given that Ni prefers to go into the γ phase rather than into the γ' phase, while Ta and Al tend to concentrate in the γ' phase, it is apparent that Ni will be rejected to the γ phase as the γ' grows and will pile up on the matrix-precipitate interface, whereas Ta and Al will be depleted of the interface, as schematically shown in Fig. 7. While this happens, the excess Ni will diffuse into the γ matrix. Therefore, if the γ' grows at a constant rate the local concentration changes would be associated with the interface. These local concentration differences will disperse as the growth of the γ' precipitate slows down. However, when the γ' precipitates approach each other the narrow γ layer in between them will rapidly become saturated with Ni, since extra Ni atoms in this region become increasing difficult to diffuse away from this thin γ layer and have to diffuse into the matrix γ along the interfaces in the slot of the phase boundary. In order to induce coalescence along $\langle 010 \rangle$ directions due to elastic interaction effects, elemental redistribution in the thin layer is required and short-range ordering of the interphase layer will be encouraged which will necessarily be in phase with only one of the γ' long-range ordered particles. For this reason, it is the interface between a thin interphase layer and one of the γ' precipitates which is associated with an APB and which would give rise to sites for which the excess Ni must have a lower free energy. When the material is quenched from high temperature (such as 1000 °C in present study), the Ni excess may be 'frozen in' and cause lattice contraction across the APB as a lattice parameter of pure Ni ($a_{Ni} = 3.52$ Å) is slightly smaller than that of Ni–12.8Al–2.4Ta alloy ($a_{\gamma} = 3.59$ Å). Therefore, it is possible to infer that the lattice shift across the APB interface can be ascribed to Ni interfacial segregation.

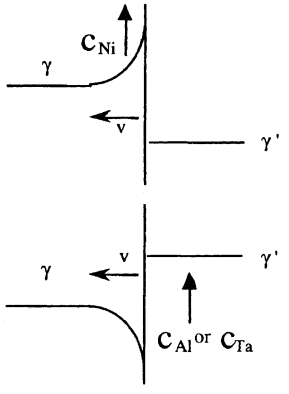

Fig. 7. Composition changes in a γ/γ' alloy caused by interface migration.

5. Conclusions

Interfacial segregation was systematically studied in the Ni–12.8Al–2.4Ta model alloy quenched after annealing at 1000 °C for 8 days. The following conclusions are derived from the results observed in this study:

1. The digitized 1D fringe profile in the thin interphase layer between the merging γ' precipitates showed that, as a result of the γ' coarsening associated with an APB, the thin layer exhibits a short-range ordering structure, although the composition is still very different from that of γ'.
2. HREM observation confirmed that coherency existed in the d_{100} fringe spacing along the interface between a thin interphase layer and the γ' precipitates, while the lattice shift across the APB was quantified as $\sim 10\%$ contraction of the d_{010} spacing using regressional analysis.
3. The excellent agreement between the magnitude of R measured using computer simulations and that measured from an HREM image using regressional analysis highlights both the influence of the bounding partial dislocation on an APB fault fringe contrast and the advantages of the qualitative measurement of a lattice shift due to segregation.
4. Interfacial segregation has been successfully identified for the first time at an APB fault interface in γ/γ' alloys. The lattice shift across the APB can be reasoned to be caused by Ni segregation to the APB interface between the thin interphase layer and one of the merging γ' precipitates due to diffusion-controlled interface migration and elastic interaction effects.

Acknowledgements

The authors are grateful for the financial support of Institute of Nuclear Energy Research (INER) and the technical supports in the Cambridge University.

References

[1] J.K. Tien, S.M. Copley, Metall. Trans. 2 (1971) 215.
[2] R.A. Mackay, M.V. Nathal, Acta Metall. 38 (1990) 993.
[3] C.Y. Chen, R.E. Dunin Borkowski, W.M. Stobbs, Inst. Phys. Conf. Ser. 138 (1993) 409.
[4] R. Schäublin, P. Stadelmann, Mater. Sci. Eng. A164 (1993) 373.
[5] A.K. Head, P. Humble, L.M Clarebrough, A.J. Morton, C.T. Forwood, Computed Electron Micrograph and Defect Identification, North Holland, Amsterdam, 1973.
[6] K.J. Hemker, M.J. Mills, Philos. Mag. 68 (1993) 305.
[7] R.E. Dunin Borkowski, W.M. Stobbs, Ultramicroscopy 72 (1998) 199.
[8] T. Miyazaki, K. Nakamura, H. Mori, J. Mater. Sci. 14 (1979) 1827.

[9] N. Matan, D.C. Cox, C.M.F. Rae, R.C. Reed, Acta metall. 47 (1999) 2031.
[10] C.Y. Chen, Ph.D. thesis, University of Cambridge, UK, 1995.
[11] T.M. Pollock, A.S. Argon, Acta metall. 42 (1994) 1859.
[12] D.A. Grose, G.S. Ansell, Metall. Trans. 12 (1981) 1631.
[13] A.F. Giamei, D.D. Pearson, D.L. Anton, Proceedings of Mater. Res. Soc. Symposium. on High Temperature Ordered Intermetallic Alloys, vol. 39, Pittsburgh, PA, 1985, p. 293.
[14] F.M. Ross, W.M. Stobbs, Phil. Mag. 1 (1991) 37.
[15] G.J. Wood, W.M. Stobbs, D.J. Smith, Phil. Mag. 50 (1984) 375.